Composites Part B 192 (2020) 107990

Contents lists available at ScienceDirect

Composites Part B

journal homepage: www.elsevier.com/locate/compositesb

Multifunctional epoxy composites with highly flame retardant and effective electromagnetic interference shielding performances

Wenwen Guo [a], Yuyu Zhao [b], Xin Wang [a,*], Wei Cai [a], Junling Wang [a], Lei Song [a], Yuan Hu [a,**]

[a] State Key Laboratory of Fire Science, University of Science and Technology of China, 96 Jinzhai Road, Hefei, Anhui, 230026, PR China
[b] School of Urban Development and Environmental Engineering, Shanghai Second Polytechnic University, Shanghai, 201209, PR China

ARTICLE INFO

Keywords:
Epoxy composites
Carbon foam
Flame-retardant
Electromagnetic interference shielding

ABSTRACT

Multifunctional epoxy composites with low flammability, high ablation resistance, superior electrical conductivity and outstanding electromagnetic interference (EMI) shielding performances are prepared by a two-step procedure. The first step involves pyrolysis of lignin-resorcinol-glyoxal pre-polymer into carbon foams, while the second step is infiltrating flame retardant epoxy resins (FREP) into the highly porous carbon foams. SEM images show that the three-dimensional network microstructure of carbon foams is integrally preserved during infiltration by the epoxy resins, which could serve as an effective pathway for electron transport. For the flame-retardant carbon foam/epoxy (FREP-CF) composite, a UL-94 V-0 classification is achieved. In the cone calorimeter measurement, the peak heat release rate and the total heat release of the FREP-CF composite are reduced by 64% and 37%, respectively, compared to those of the original epoxy resin. The FREP-CF composite can resist approximately 1000 °C flame for 10 min with the temperature on the back side lower than 200 °C, which is much better than the EP-CF composite. Additionally, a notable electrical conductivity of 216 S/m and a superior EMI shielding effectiveness of 33.5 dB are achieved for the FREP-CF composite. This multifunctional epoxy composite enables it a promising candidate for electronics, aerospace and transportation applications.

1. Introduction

As one of the most important thermosetting polymers, epoxy resins (EPs) possess good mechanical strength and stiffness, superior adhesive, outstanding solvent resistance and dimensional stability after curing [1–5][62]. Owing to these fascinating comprehensive performances, EPs have been applied in a wide variety of industrial applications in the realms of electronics, aerospace and transportation [6–10][63]. However, these application fields require several specific demands like flame retardancy, ablation resistance, electrically conductive and electromagnetic interference (EMI) shielding performances in addition to the intrinsic properties of EPs. It is thereby imperative to modify EP matrix to develop multi-functional epoxy composites for various applications.

One conventional methodology for development of epoxy composites is dispersing functional nano-particles or additives into epoxy matrix. For example, in order to improve the flame retardancy of EPs, various organic additives such as phosphorus- [2], nitrogen- [11], silicon- [12], boron-containing [13] compounds and inorganic nano-particles including graphene [14–16], layered double hydroxide [17], carbon nanotubes [18], boron nitride [19,20], zirconium phosphate [21], or their hybrids [22] have been added into epoxy matrix; for the EMI shielding enhancement, a wide variety of nano-particles such as single-walled carbon nanotube [23], multi-walled carbon nanotube-Fe_3O_4@Ag composite [24], graphene [25], reduced graphene oxide-carbon fiber composite [26], and reduced graphene oxide/-Fe_2O_3/carbon fibers mixture [27], have been incorporated to EPs. Theoretically, the enhancement in the EMI shielding performance relates closely to the formation of electrically conductive networks which usually requires high loading of nano-particles. Considering that such high loading of nano-particles is used, aggregation of the nano-particles is difficult to be avoided. Additionally, the high loading of nano-particles also negatively affects the thermal stability of the resultant epoxy composites [16].

Construction of the continuous three-dimensional networks within the polymer-based composite materials emerges as a promising strategy to overcome the aforementioned restriction on dispersibility of nano-particles in polymer matrix [28]. Generally, a two-step procedure is employed to fabricate such composite materials with the continuous

* Corresponding author.
** Corresponding author.
E-mail addresses: wxcmx@ustc.edu.cn (X. Wang), yuanhu@ustc.edu.cn (Y. Hu).

https://doi.org/10.1016/j.compositesb.2020.107990
Received 12 November 2019; Received in revised form 3 March 2020; Accepted 18 March 2020
Available online 21 March 2020

three-dimensional networks: (1) Construction of continuous networks with open pore, followed by (2) infiltration of polymers into the voids of the continuous networks. For the first step, carbon foams made from graphene, carbon fiber, carbon nanotube and their hybrids have been considered to be ideal EMI shielding materials owing to porous structure, light weight, tunable electrical conductivity and absorption property [29]. Recently, utilization of low-cost and renewable precursors for fabrication of carbon foams has received great attentions in terms of economical and environmentally friendly concerns. Lignin, as the most abundant aromatic natural polymer, contains very high carbon content (above 60%) and a large number of phenolic hydroxyl groups [30], which is an attractive and sustainable precursor for carbon foams. Moreover, due to its structural similarity with phenol and resorcinol, lignin has been considered as a promising natural alternative to synthetic phenolic compounds in preparation of phenolic resins [31], which could be applied as sustainable precursor for fabrication of carbon foams.

Regarding the application of carbon foam/polymer composites as EMI shielding materials, Chen et al. reported that epoxy nanocomposites reinforced with three-dimensional carbon nanotube sponge exhibited a relatively high electrical conductivity of 148 S/m and a superior EMI shielding effectiveness of about 33 dB, which is much better than those for epoxy composites filled with conventional carbon nanotubes [28]. Chen et al. also prepared three-dimensional graphene aerogel reinforced epoxy nanocomposite which exhibited a high electrical conductivity of 73 S/m and an excellent EMI shielding effectiveness of 35 dB [32]. Kim et al. fabricated non-oxidized graphene flake aerogel−epoxy composite with a remarkable electrical conductivity of 122.6 S/m [33]. Chen et al. developed a lightweight and flexible graphene foam/polydimethylsiloxane composite with an EMI shielding effectiveness of 30 dB and a specific shielding effectiveness of 500 dB cm^3/g [34]. Zeng et al. constructed porous multi-walled carbon nanotube/waterborne polyurethane composites which displayed an EMI shielding effectiveness of more than 50 dB and a specific shielding effectiveness of 1148 dB cm^3/g [35]. These previous studies demonstrate the superior reinforcing effectiveness of continuous three-dimensional networks over conventional nano-particles. Most of such studies focus on improvement in one or two specific performances; however, multifunctional epoxy composites with simultaneously enhanced flame retardancy, ablation resistance, electrically conductive and EMI shielding performances are more desired for specific applications in electronic devices, aerospace, machinery manufacturing, automobile and marine systems [28].

Iminophosphoranes are one family of organophosphorus compounds with a common structural feature P═N, which have been well known as ligands for homogeneous catalysis [36]. However, until now, it is rarely reported on utilization of iminophosphoranes as flame retardant additives. In this work, one kind of N-phosphorylated iminophosphorane was selected as flame retardant because it contains both phosphorus and nitrogen elements which could create synergistic effect in enhancing flame retardancy. Additionally, N-phosphorylated iminophosphorane is a kind of liquid flame retardant, which is favorable for blending with EP resin.

This work aimed to integrate low flammability, high ablation resistance, superior electrical conductivity and outstanding EMI shielding performances into epoxy composites. For this purpose, a continuous three-dimensional carbon foam derived from renewable lignin was chosen to enhance electrical conductivity and EMI shielding of EP, while N-phosphorylated iminophosphorane was incorporated to improve flame retardancy and ablation resistance. Carbon foam was prepared by pyrolysis of lignin-resorcinol-glyoxal precursor using flexible polyurethane foam (FPUF) as the template. The influence of the pyrolyzed temperature and the reactant concentration on the morphology and structure of the carbon foam was investigated. The carbon foam with superior combined properties was selected to fabricate epoxy composites through vacuum-assisted infiltration technology. The flame retardancy, ablation resistance, electrical conductivity and EMI shielding performances of the resultant carbon foam reinforced epoxy composites were characterized by limiting oxygen index (LOI), UL-94 vertical burning test, cone calorimeter, fire resistance test, thermogravimetric analysis, and electrical conductivity and EMI shielding measurements.

2. Experimental

2.1. Materials

Polyether-based FPUF with a density of about 20 kg/m^3 was kindly provided by Lv'yuan New Material Company (Jiangsu, China). Alkali lignin was purchased from Sigma-Aldrich, USA. Resorcinol, glyoxal (~40% aqueous solution), ethanol, sodium hydroxide, diphenyl phosphite, trimethyl phosphite, acetonitrile, carbon tetrachloride, chloroform and magnesium sulfate anhydrous were purchased from Shanghai Aladdin Bio-Chem Technology Co., Ltd (Shanghai, China). Sodium azide was supplied from Merck Schuchardt OHG (Darmstadt, Germany). Tetraglycidyl dimethylenedianiline (TGDDM) and methyl tetrahydrophthalic anhydride (MTHPA) were provided by Shanghai Huayi group company (Shanghai, China). All chemical reagents were used without purification.

2.2. Samples preparation

2.2.1. Synthesis of N-phosphorylated iminophosphorane ($(Ph_2O)(O)P–N═P(OMe)_3$)

Diphenyl phosphite (46.8 g, 0.2 mol), trimethyl phosphite (24.8 g, 0.2 mol), sodium azide (19.5 g, 0.3 mol) and acetonitrile (100 mL) were charged into a three-necked round-bottom flask fitted with a condenser, mechanical stirrer, and a thermometer. The mixture was heated to 80 °C and then carbon tetrachloride was added dropwise during 1 h. When the release of nitrogen ceased, the reaction continued for another 2 h. The solvent was subsequently removed by rotary evaporator. The crude product was re-dissolved in chloroform and washed with water three times. The organic layer was dried by magnesium sulfate anhydrous followed by the removal of the solvent once again. FT-IR (KBr, cm^{-1}): 3043 (C_{aryl}-H), 2855 (C_{alkyl}-H), 1592, 1490 (C_{aryl} = C_{aryl}), 1292 (P═N), 1196 (P═O), 1048 (=C_{aryl}-H in-plane def.). ^{1}H NMR (400 MHz, $CDCl_3$, ppm): 3.39–3.93 (m, 9H), 6.77–7.35, (m, 10H).

2.2.2. Synthesis of lignin-based carbon foam

First, lignin-resorcinol-glyoxal (LRG) pre-polymer was prepared under the basic condition by polycondensation of lignin, resorcinol and glyoxal using sodium hydroxide as catalyst. Typically, in a three-necked round-bottom flask, 5.05 g lignin, 24.58 g glyoxal (~40% aqueous solution), 5.05 g resorcinol and 0.2 g sodium hydroxide were dissolved in 65 ml deionized water and stirred at 60 °C for 4 h. The mixture was subsequently transferred to a beaker and a piece of FPUF was immersed to the mixture and squeezed several times to ensure that the FPUF was filled with the lignin-resorcinol-glyoxal pre-polymer. The treated FPUF was totally dried in an oven at 80 °C for 12 h. The LRG-coated FPUF was placed in a furnace under argon atmosphere, and then heated from ambient temperature to 900 °C at a rate of 2 °C/min. The sample was maintained at 900 °C for 2 h in order to complete the carbonization and then cooled naturally to ambient temperature. In order to investigate the influence of the reactant concentration and the pyrolyzed temperature on the property of the samples, a series of the carbon foams were prepared using a similar method and the experimental condition is listed in Table S1.

2.2.3. Infiltration of epoxy into carbon foam

TGDDM (50 parts) was firstly blended with $(Ph_2O)(O)P–N═P(OMe)_3$ (10 parts) and MTHPA hardener (40 parts) to obtain a uniform liquid epoxy resin. The carbon foam reinforced flame-retardant epoxy composites were fabricated by a vacuum-assisted infiltration technology. Typically, the carbon foam was placed at a mold with an inlet tube and

an outlet tube. The mold was then sealed in a vacuum bag with the closed inlet tube by a clamp. The vacuum bag was degassed for 10 min by a pump which was connected to the outlet tube, and the inlet tube was put into the pre-mixed epoxy resin and then the clamp was removed. The vacuum forced the epoxy resin to infiltrate into the mold through a preset inlet tube. After the carbon foam in the mold was completely filled with the epoxy, both the inlet tube and the outlet tube were closed by the clamps. Finally, the vacuum bag with the carbon foam reinforced epoxy composite was placed in an oven to obtain a cured product. The curing procedure was 100 °C for 2 h, 150 °C for 2 h and 180 °C for 2 h. For comparison, the carbon foam reinforced epoxy composites were fabricated by a similar method just without adding the $(Ph_2O)(O)P–N{=}P(OMe)_3$.

2.2.4. Preparation of reference epoxy samples

Reference epoxy and flame retardant epoxy samples were prepared as below: TGDDM (50 parts) was firstly blended with $(Ph_2O)(O)P–N{=}P(OMe)_3$ (10 parts) and MTHPA hardener (40 parts) to obtain a uniform liquid epoxy resin, and subsequently poured into a polytetrafluoroethylene mold. The samples were cured at 100 °C for 2 h, 150 °C for 2 h and 180 °C for 2 h. For comparison, the unmodified epoxy samples were obtained by a similar procedure just without adding the $(Ph_2O)(O)P–N{=}P(OMe)_3$.

2.3. Characterization

Chemical structure was characterized by a Fourier-transform infrared spectrometer (FTIR, ThermoFisher Scientific, Nicolet 6700, USA) using a KBr disc containing finely ground samples (1%), and by a nuclear magnetic resonance (NMR) spectroscopy (Bruker AVANCE AV400, Switzerland) with a $CDCl_3$ as solvent. For FTIR of each specimen, 32 scans were recorded in the spectral range from 400 to 4000 cm^{-1} in the transmittance mode with a resolution of 0.5 cm^{-1}.

Morphological characterization was performed by field-emission scanning electron microscope (SEM, Hitachi SU8200, Japan) equipped with an Energy Dispersive X-ray spectroscopy analysis (EDX, Oxford, UK). Samples for SEM analyzes were sputtered by a conductive gold layer prior to SEM observation.

The carbon foams and the solid residues collected after cone calorimeter measurement were analyzed by a LabRAM-HR Confocal Raman Microprobe (Jobin Yvon Instruments, France) using 514.5 nm argon ion laser.

Thermogravimetric analysis (TGA) with a heating rate of 20 °C/min was performed on a thermogravimetric analyzer (TGA Q5000IR, TA Instruments, USA) by heating approximately 5.0 mg samples to 700 °C under nitrogen or technical air atmosphere.

The electrical conductivity was determined by a four-point probe (FT-340, Ningbo rooko instruments, China). At least five times were repeated and the average value was reported.

The S parameters of the samples were measured on a vector network analyzer (AV3672, China electronics technology instruments Co., Ltd) using the wave-guide method in the frequency range from 8.2 to 12.4 GHz (X-band). The cubic sample with the size of 22.9 mm × 10.2 mm × 9.7 mm was placed into the holder prior to measurements.

The limiting oxygen index (LOI) was measured following the testing procedure described in ASTM D2863-17a standard using a HC-2 LOI tester (JiangNing Instruments, China). The size of the specimens was 100 mm in length, 6.5 mm in width and 3 mm in thickness.

The UL-94 vertical burning test was measured according to the testing procedure described in ASTM D3801-19 standard using a horizontal/vertical flame chamber (JiangNing Instruments, China). The size of the specimens was 100 mm in length, 13.0 mm in width and 3 mm in thickness.

Fire behavior was tested by means of cone calorimeter (Fire Testing Technology, UK) according to ISO 5660-1 standard. The rectangular specimens with the size of 100 mm × 100 mm × 3 mm were wrapped by aluminum foil and exposed to an external heat flux of 50 kW/m^2. The cone calorimeter measurements for each sample were repeated for three times and the average results were reported.

For the fire-resistant test, the rectangular specimens with the size of 100 mm × 100 mm × 10 mm were directly exposed to a propane/butane blow torch flame. During the fire-resistant test, one thermocouple labelled T1 was used to measure the temperature on the front side of the specimen, while another three thermocouples labelled T2-T4 were used to monitor the temperature on the back side. The infrared thermography (A655sc, FLIR Company, USA) was also utilized to capture the thermographic images of the back side.

3. Results and discussion

The multifunctional epoxy composites are fabricated by a two-step procedure, as shown in Fig. 1. The three-dimensional porous carbon foam is firstly prepared through pyrolysis of lignin-resorcinol-glyoxal pre-polymer at high temperature using flexible polyurethane foam as the template, followed by infiltration of liquid flame retardant epoxy mixture into it. From the SEM micrographs, it can be clearly seen that the original flexible polyurethane foam shows porous structure with open cells. After pyrolysis, the porous structure with open cells is well preserved for the carbon foam. For the composite material, the open cells of the carbon foams are fully filled with the epoxy resins, demonstrating this strategy by impregnating epoxy pre-polymer into a highly porous three-dimensional microstructure is feasible.

The influence of the pyrolyzed temperature on the morphology of the carbon foam was investigated using SEM, as illustrated in Fig. S1. It can be seen that the original flexible polyurethane foam shows a porous structure with open cells, and the cell wall is relatively smooth under high magnification (Fig. S1a). After pyrolysis under different temperatures, a honeycomb-like structure with open cells is well preserved for the carbon foam (Figs. S1b–S1d) which facilitates the infiltration of epoxy in the following step. Under high-magnification SEM images, the cell walls become thinner and rougher as compared to those of the original flexible polyurethane foam owing to the removal of the template. The reactant concentration on the morphological features of the carbon foams was also studied by SEM, as shown in Fig. S2. It can be found that the higher reactant concentration results in similar porous structure but much rougher cell walls.

Raman spectrometer is a powerful tool to study the graphitization degree of carbonaceous materials. The influence of the reactant concentration and the pyrolyzed temperature on the graphitization degree of the carbon foam was investigated by Raman spectrometer. Fig. 2 gives the Raman spectra of the carbon foams. It can be found that the Raman spectra of all the samples show two predominant bands at 1360 and 1598 cm^{-1}, which is called D-band and G-band, respectively. The D-band is associated with the amorphous domains consisted of disordered carbon atoms, while the G-band is assigned to the crystalline regions with graphitized carbon atoms [37,38]. The area ratio of the G-band and D-band (I_G/I_D) is usually utilized to assess the graphitization degree of carbonaceous materials [20]. The I_G/I_D value of the samples follows the order of CF-1-600 (0.34) < CF-1-750 (0.36) < CF-1-900 (0.41), indicating that the crystalline carbon structure is favorable to be formed at higher pyrolyzed temperature. Additionally, the increased reactant concentration slightly improves the I_G/I_D value of the carbon foams.

In order to evaluate the thermal stability and thermal degradation behaviors, TGA and differential TGA (DTG) thermograms of the carbon foams under air are shown in Fig. S3. The original FPUF shows a two-stage thermal degradation process: the first stage is related to the decomposition of urethane groups, while the second one is associated with the decomposition of the polyether into volatile fragments [39,40]. After pyrolysis, the thermal stability of the carbon foams is improved significantly owing to the formation of thermally stable lignin-phenol-formaldehyde resins. Furthermore, the thermal stability of the carbon foams is improved with the increment of the pyrolyzed

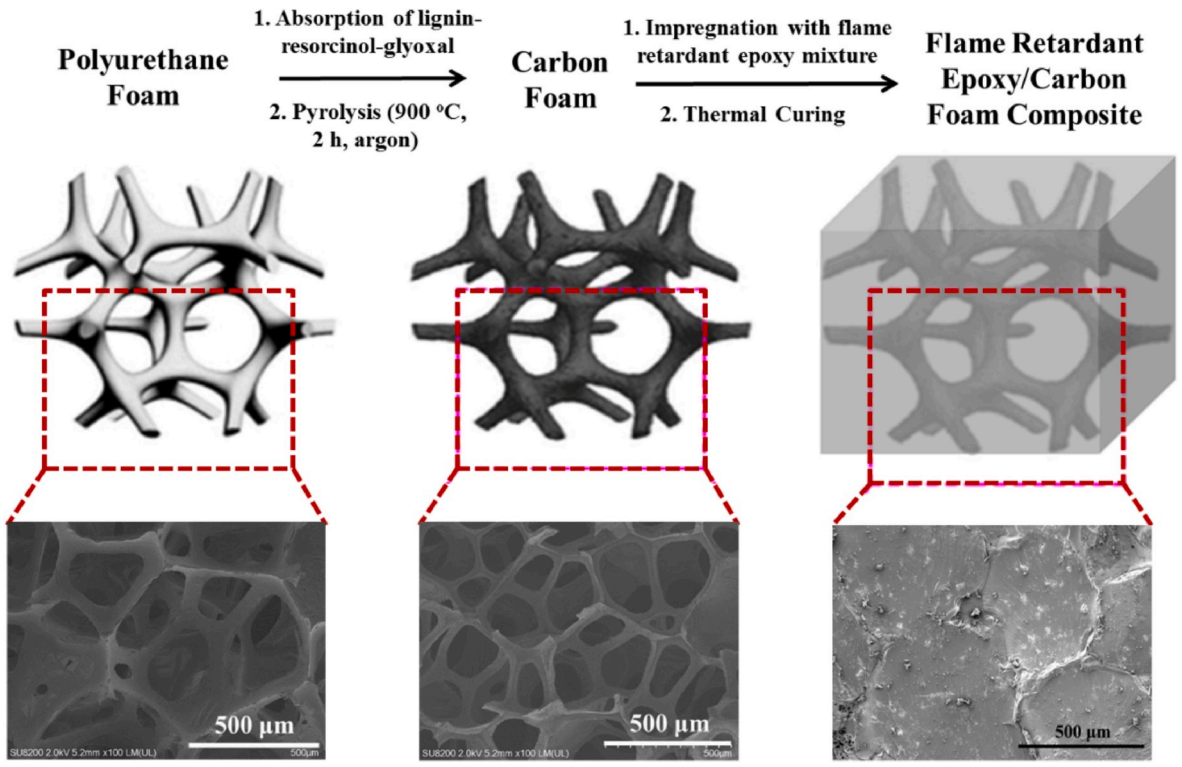

Fig. 1. Schematic Illustration of preparation of the flame retardant epoxy/carbon foam composite (Top row) and SEM micrographs of the corresponding structures (Bottom row).

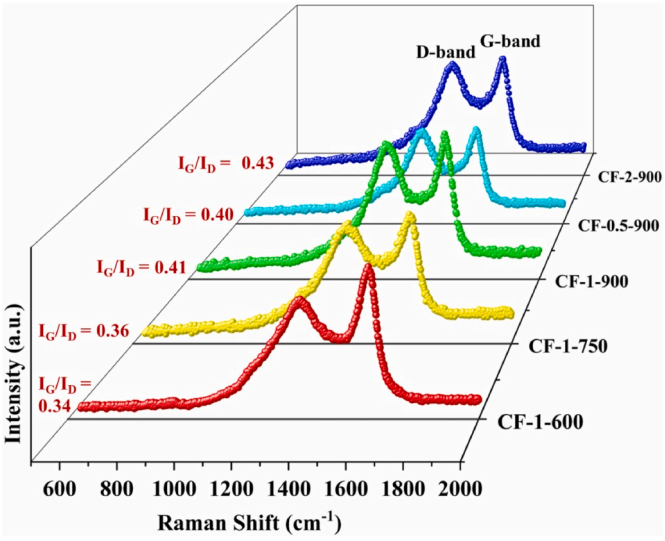

Fig. 2. Raman spectra of the carbon foams.

temperature because of the enhanced graphitization degree. In addition, the reactant concentration also affects the thermal stability of the carbon foams. The thermal stability increases as the reactant concentration rises.

Electrical conductivity plays the most important role in the reflection and absorption shielding [41]. To evaluate the influence of the pyrolyzed temperature on the electrical conductivity of carbon foams, Fig. S4 presents the electrical conductivity of the samples. It can be observed that the electrical conductivity values of carbon foams significantly enhanced with the increase of the pyrolyzed temperature. Most noticeably, the CF-1-900 presents the highest electrical conductivity of 383.0 S/m. In addition, the effect of the reactant concentration on the electrical conductivity of the carbon foams is also investigated. The electrical conductivity value increases from 191.3 S/m for CF-0.5-900 to 383.0 S/m for CF-1-900, and no further increase in the electrical conductivity (366.2 S/m) for the CF-2-900 is observed. These results indicate that the increase in the pyrolyzed temperature and the reactant concentration result in a noticeably improved electrical conductivity value for carbon foams. This is generally ascribed to that the more densely conductive network is formed when the pyrolyzed temperature and the reactant concentration increase. So, the CF-1-900 is the optimal formulation to form a densely conductive network with the best conductivity.

SEM is employed to assess the microstructures of the epoxy and its carbon foam composites. The original epoxy thermoset shows a mirror-like fractured surface, indicating a brittle nature of the epoxy matrix (Fig. 3a and b). For the EP-CF (Fig. 3c and d) and the FREP-CF (Fig. 3e and f) composites, the open cells of the carbon foams are filled with the epoxy resins, demonstrating this strategy by impregnating epoxy pre-polymer into a highly porous three-dimensional microstructure is feasible. Furthermore, the continuous three-dimensional microstructure is well preserved during infiltration of the epoxy pre-polymer into the carbon foam. Consequently, the physically-interconnected microstructure facilitates the electron transport to form an electrically conducting network.

The electrical conductivity of the FREP-CF composite is determined to be 216.0 S/m by a four-probe method. The superior electrical conductivity of the FREP-CF composite is also proved by the electrical test (Fig. 4a). It can be seen that the LED lamp lights when switching on the FREP–CF–connected circuit. Fig. 4b shows the EMI shielding effectiveness including the total shielding effectiveness (SE_T), the absorption shielding effectiveness (SE_A) and the reflection shielding effectiveness (SE_R) of the pristine EP and the FREP-CF composite. It can be observed that the pristine EP is almost transparent to electromagnetic interference and shows nearly no shielding ability to electromagnetic waves in the frequency of 8.2–12.4 GHz. Strikingly, for the FREP-CF composite system, the SE_T is dramatically increased to approximately 33.5 dB, which

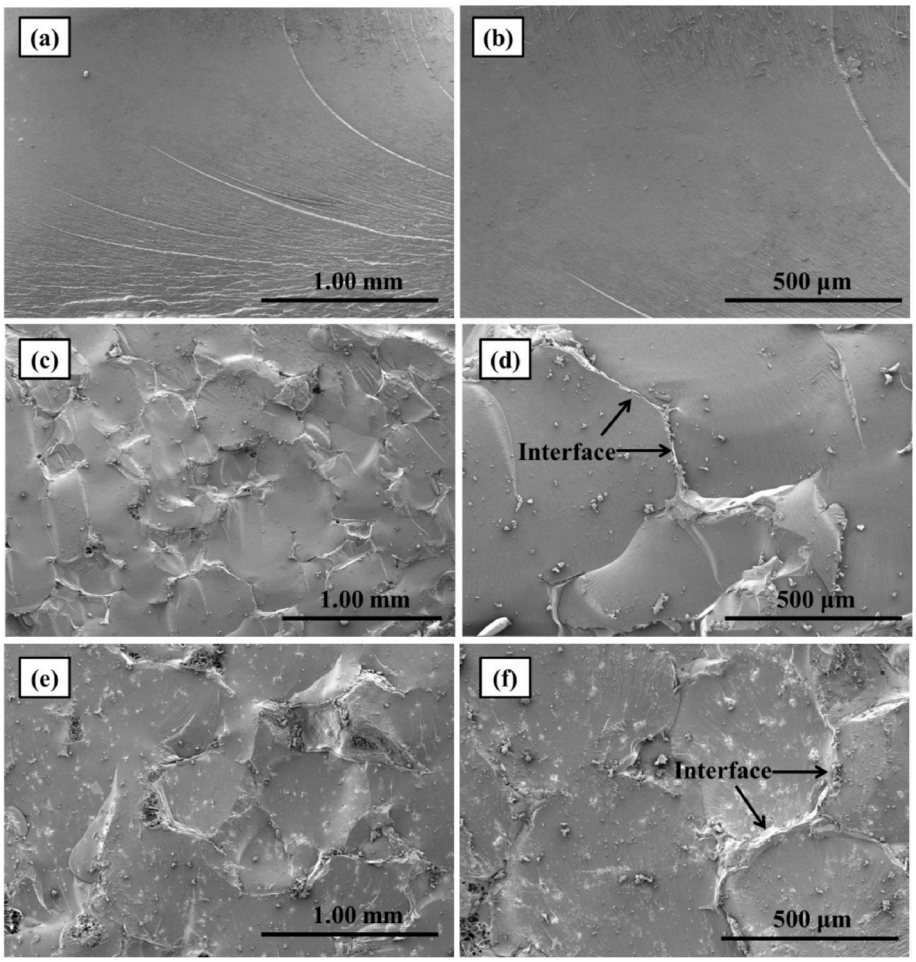

Fig. 3. SEM images of (a, b) EP, (c, d) EP-CF and (e, f) FREP-CF under different magnifications.

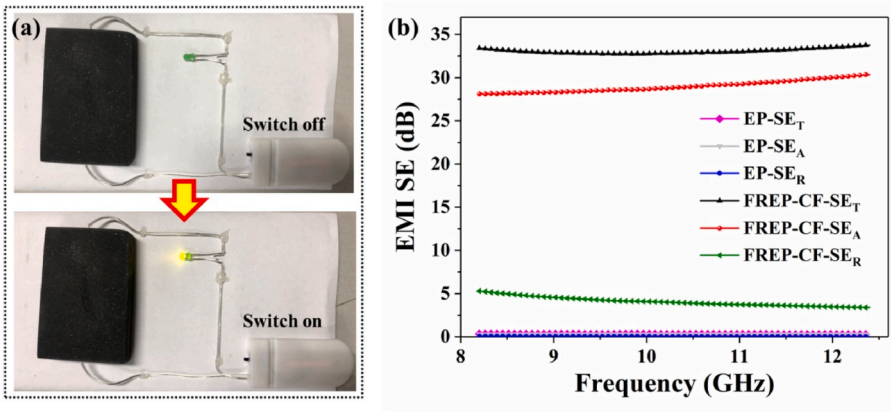

Fig. 4. (a) Images illustrating that the FREP-CF connected circuit, and (b) EMI shielding performance of the pristine EP and the FREP-CF composite.

is far more than the commercial standard (20 dB) for electromagnetic interference shielding materials. Under these circumstances, above 99.9% of the electromagnetic waves can be blocked. In addition, the average SE_A value of the FREP-CF composite is 29.4 dB which is much higher than its average SE_T value of 4.1 dB, implying that the absorption shielding is the prominent shielding mechanism of FREP-CF composites which is in good consistent with the results discussed above. The difference between absorption shielding effectiveness and reflection shielding effectiveness with increasing the pyrolyzed temperature and the reactant concentration is attributed to the interfacial polarization of the FREP-CF composite. The reflection shielding is usually the original mechanism of the electromagnetic radiation incident, owing to the free electrons on the surface of the shielding material interacted with the electromagnetic radiation [28]. The secondary mechanism of the EMI shielding is generally the absorption shielding, which is the interaction between the electromagnetic fields in the radiation and the electric dipoles inside the shielding network [24,43].

A comparison of the EMI shielding performance of the FREP-CF composite in this work with its counterparts in previous studies is shown in Table 1. Compared to the conventional strategy through

incorporating randomly dispersed graphene, carbon fiber and carbon nanotubes in previous studies [23,24,44–51], the carbon foam with well preformed three-dimensional network and more densely conductive pathway is relatively more efficient in enhancing the EMI shielding performance of epoxy composites. By contrast, the FREP-CF composite containing comparatively low loading (6 wt%) of carbon foam in this work exhibits relatively higher electrical conductivity (216 S/m) and superior EMI shielding performance (33 dB) in X band, suggesting that it is one of the most promising high-performance EMI shielding materials.

The flame-retardant property of the samples was assessed by the LOI and UL-94 results, as summarized in Table 2. The control sample EP has a relatively low LOI value of 22.0%, implying a highly inflammable material, which is also proved by no rating and dripping in the UL-94 vertical burning test. The addition of 10 wt% of N-phosphorylated iminophosphorane into EP increases the LOI value to 29.0% as well as a V-0 rating in the UL-94 vertical burning test. For the EP-CF composite, the LOI value is 23.0% and no rating and dripping is observed in the UL-94 vertical burning test, indicating the presence of the carbon foam cannot inhibit flame spread. By comparison, the LOI value of the FREP-CF composite increases to 29.5% accompanying with a UL-94 V-0 rating, demonstrating excellent flame-retardant property. The improved flame retardancy of the FREP and FREP-CF composites is related to that the thermal degradation of the N-phosphorylated iminophosphorane generates, on the surface, a protective layer which inhibit the flame spread effectively.

The combustion behaviors were also investigated by the cone calorimeter, which could well reflect fire hazards of polymers in bench scale measurement [52–54]. The fire-related characteristics obtained from cone calorimeter including the time to ignition (t_{ig}), the peak heat release rate (PHRR), the total heat release (THR), the residue yield and the time to PHRR (t_{PHRR}) is summarized in Table 2. Fig. 5 illustrates the heat release rate (HRR) as a function of the time curves. After ignition, the original EP burns fiercely with an intense HRR peak of 1199 kW/m^2. The addition of 10 wt% of N-phosphorylated iminophosphorane decreases the PHRR to 366 kW/m^2, corresponding to a 69% reduction. Furthermore, the HRR curve of the FREP becomes broaden with a "platform" stage. Generally, the phosphorus-containing flame retardants cause the earlier degradation of polymers to trigger the char formation that serves as a physical barrier to suppress the heat release. The formation of this char layer accounts for the appearance of the "platform" stage in the HRR curve. With increasing the exposure time to heat irradiation, the char layer however collapses owing to the thermal oxidative degradation, resulting in a subsequent higher HRR peak. The EP-CF and FREP-CF also exhibit a broaden HRR curves that is similar to the FREP, since the carbon foam is an inter-connected network consisted of lots of char layers that could inhibit the heat release rate during combustion. The PHRR is declined by approximately 51% and 64% in EP-CF and FREP-CF, respectively.

Table 1
Comparison of EMI shielding performance of FREP-CF composite in this work with epoxy composites in previous reports.

Epoxy composites	Content	Conductivity (S/m)	EMI SE (dB)	Frequency (GHz)	Ref.
EP/MWCNT-Fe_3O_4@Ag	15 wt%	28	35	8.2–12.4	[24]
EP/F-MWCNTs/MnZn ferrite	4 vol%	–	17	8.2–12.4	[44]
EP/SWCNTs	15 wt%	20	25	10	[23]
EP/graphene	15 wt%	10	21	8.2–12.4	[45]
EP/CB	30	–	44	1–10	[46]
EP/TGO/SCI	33 wt%	–	32	8.2–12.4	[47]
EP/GNPs/rGO	20.5 wt %	179	51	8.2–12.4	[48]
EP/GCF/MG3	9 wt%	11	37	8.2–12.4	[49]
EP/F-MWCNT	5 wt%	0.03	20.5	8.2–12.4	[50]
EP/SWCNT	0.6 wt%	5×10^{-4}	12.8	8.2–12.4	[51]
FREP-CF	6 wt%	216	33	8.2–12.4	This work

Table 2
LOI values, UL-94 vertical burning behaviors and cone calorimeter data of the control EP, the FREP, the EP-CF and the FREP-CF samples under 50 kW/m.^{2}.

Samples	EP	FREP	EP-CF	FREP-CF
LOI (%) ± 0.5	22.0	29.0	23.0	29.5
UL-94	No Rating	V-0	No Rating	V-0
t_{ig} (s) ± 1	37	29	23	21
PHRR (kW/m^2) ± 5%	1199	366	588	436
THR (MJ/m^2) ± 3%	85.8	66.3	83.2	54.3
Residue (%) ± 5%	7.0	26.4	9.2	31.3
t_{PHRR} (s) ± 1	89	159	117	113
FIGRA (kW/m^2·s)	13.5	2.3	5.0	3.8

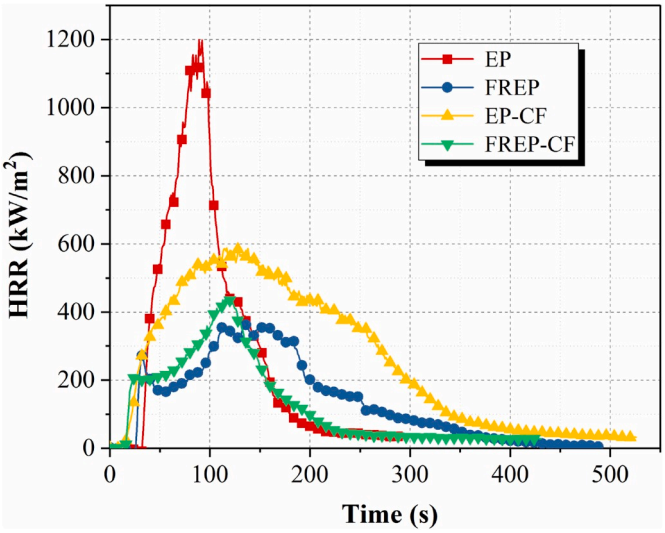

Fig. 5. The heat release rate (HRR) as a function of time curves of the samples.

The THR as a function of the time curves are plotted in Fig. 6. Considering that the THR is associated with the total amount of fuel released and the combustion efficiency of the fire, a decrease in the THR is expected for flame retardant materials. Specifically, this parameter is

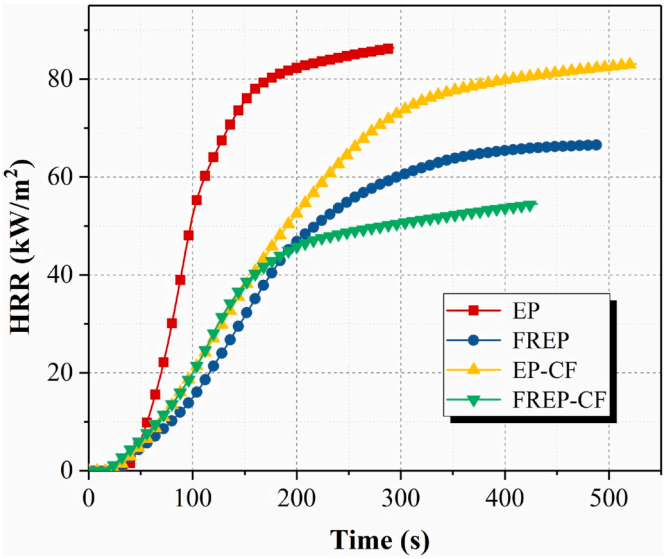

Fig. 6. The total heat release (THR) as a function of time curves of the samples.

reduced by 23% in FREP, indicating less amount of fuel evolved into flame zone. The high char yield (26.4%) of the FREP after flameout also provides evidence that a smaller number of solid polymers pyrolyzes into flammable volatiles (fuel). The phenomenon that no significant difference between the THR values of EP and EP-CF suggests the carbon foam does not significantly affect the total amount of fuel released, as also evidenced by the similar char yield between them (Table 2). By comparison, the THR value is reduced by 37% in FREP-CF owing to the much higher char yield (31.3%).

The mass loss as a function of the time curves are plotted in Fig. 7. It can be observed that the original EP has the faster mass loss rate compared to the other samples, because it has poor resistance to thermal oxidative degradation (Fig. S5a). The original EP shows a relatively low char residue (7.0%) after cone calorimeter test. For the EP-CF, the presence of carbon foam in the composite could resist to thermal oxidative degradation at the beginning of combustion, but the char loses its protective ability at higher temperature owing to the oxidation (Fig. S5b). The FREP exhibits a much slower mass loss rate, since the N-phosphorylated iminophosphorane could improve the thermal oxidative resistance of the char formed (Fig. S5c), leaving a high char yield (26.4%) after combustion. The combination of N-phosphorylated iminophosphorane and carbon foam further improves the char yield (31.3%) owing to formation of a continual and compact char layer with good thermal stability (Fig. S5d).

Another derivative parameter called the fire growth rate index (FIGRA) is calculated from the ratio of PHRR/t_{PHRR} to assess the fire risk of materials [55–58]. As observed in Table 2, the original EP has a FIGRA value of 13.5 kW/(m^2·s), implying a fast flame spread risk. The FIGRA values of the FREP, the EP-CF and the FREP-CF are reduced to 2.3, 5.0, 3.8 kW/(m^2·s), respectively, indicating a suppressed fire risk.

The time-dependent fire-resistant test of the EP-CF and the FREP-CF composites was performed by monitoring the temperature when the sample was directly exposed to a flame of a propane/butane blow torch (Fig. 8a). The temperature of the flame generated by the blow torch is approximately 1000 °C, which is measured by the thermocouple (T1) on the front side of the sample (Fig. 8b and c). Subjecting the EP-CF sample to the flame causes a slow increase of the back-side temperature up to 200 °C after 4 min followed by an abrupt increase to more than 500 °C because the EP-CF is burnt out (Fig. 8b). By contrast, the exposure of the FREP-CF to the flame gives rise to a slow increase of the back-side temperature, but the back-side temperature does not exceed 200 °C even after 10 min (Fig. 8c). The back-side temperature of the EP-CF and the FREP-CF samples were also monitored by the Infrared thermography

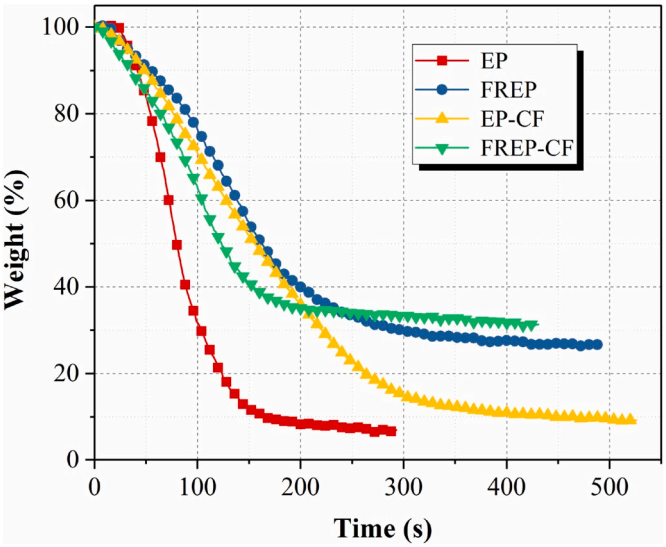

Fig. 7. The weight loss as a function of time curves of the samples.

(Fig. 8d), which shows the similar results to the thermocouples (T2-T4). After fire resistant test, some part of the EP-CF is consumed by the flame causing a hole on the residue, while the FREP-CF still maintains its structural integrity after being exposed to the flame for 10 min (Fig. 8e). It can be seen more clearly from the side view of the residues that a slightly intumescent char layer is formed and covered on the sample which could shield the underlying sample from attack by the flame. The addition of N-phosphorylated iminophosphorane promotes the carbonization that is responsible for the enhanced ablation resistance.

Fig. 9 gives TGA and differential TGA (DTG) profiles of the samples under nitrogen and air atmosphere. Under nitrogen atmosphere, the samples show a major mass loss stage ranging from 300 to 500 °C (Fig. 9a), corresponding to the decomposition of cross-linked epoxy networks to volatile fragments. In the EP-CF, it can be seen that the presence of the carbon foam has slight influence on the initial thermal degradation temperature. While for the FREP and the FREP-CF, a more significantly reduced initial degradation temperature is observed. The addition of N-phosphorylated iminophosphorane results in the shift of initial degradation to lower temperature, because of the earlier degradation of the phosphorus-containing flame retardant which is essential to trigger the char formation. At the end of the decomposition stage, the char yield of the samples follows the sequence of EP (7.7%) < EP-CF (11.9%) < FREP (22.8%) < FREP-CF (29.4%). It can be found that the incorporation of the N-phosphorylated iminophosphorane leads to much higher char yield owing to the formation of P- and N-complexed char with better thermal stability. Under air atmosphere, the samples show a major mass loss stage ranging from 300 to 430 °C (Fig. 9b), because the presence of oxygen accelerates the degradation of the cross-linked epoxy networks. There is further another stage occurring from 530 to 700 °C in air due to the oxidative processes of the char residues. The original EP has almost no residue (0.7%) at 750 °C. The EP-CF also shows very low char yield (1.7%), implying the poor thermal oxidative resistance of the carbon foam. Similar to nitrogen atmosphere, the FREP and the FREP-CF exhibit a relatively high char yield of 17.5% and 16.9%, respectively, demonstrating good charring ability of N-phosphorylated iminophosphorane as well as good thermal stability of the char formed. From the DTG curves, it can be further observed that the maximum mass loss rate of the FREP-CF is much lower than that of the original EP, which could be attributable to the higher char yield that serves as a barrier to slow down the evolved volatiles. This phenomenon agrees well with the cone calorimeter results.

The flame-retardant property is related closely with the quality of char residues during combustion. The Raman spectra of the char residues of the samples are given in Fig. S6. The I_G/I_D value of the samples follows the sequence of EP (0.28) ≈ EP-CF (0.29) < FREP (0.42) ≈ FREP-CF (0.41). It can be found that the addition of N-phosphorylated iminophosphorane is crucial to improve the graphitization degree of the chars, whereas the presence of carbon foam affects the graphitization slightly. The higher I_G/I_D value (the higher graphitization degree) means the better thermal oxidative resistance of the chars which accounts for higher char yield of FREP and FREP-CF in the TGA and the cone calorimeter measurements.

The morphological information of the char residues after cone calorimeter tests were observed SEM, as depicted in Fig. 10. The original EP displays little char yield with a lot of holes on the surface of the outer char (Fig. 10a-o) as well as many cracks in the inner char (Fig. 10a–i). The oxygen can permeate into the underlying matrix and the decomposition volatile products can escape from the decomposition zone to the flame through these holes and cracks, which is not helpful for flame inhibition. By contrast, the outer char residue of the FREP shows a continual and compact structure (Fig. 10b-o), while the inner char residue presents a honeycomb-like structure that implies the gasification of the inner polymers during combustion (Fig. 10b–i). This structured char means the decomposition volatile products inside are restrained by the outer char effectively, as evidenced by the closed bubbles formed on the surface of the outer char (as indicated by the red circles) (Fig. 10b-o).

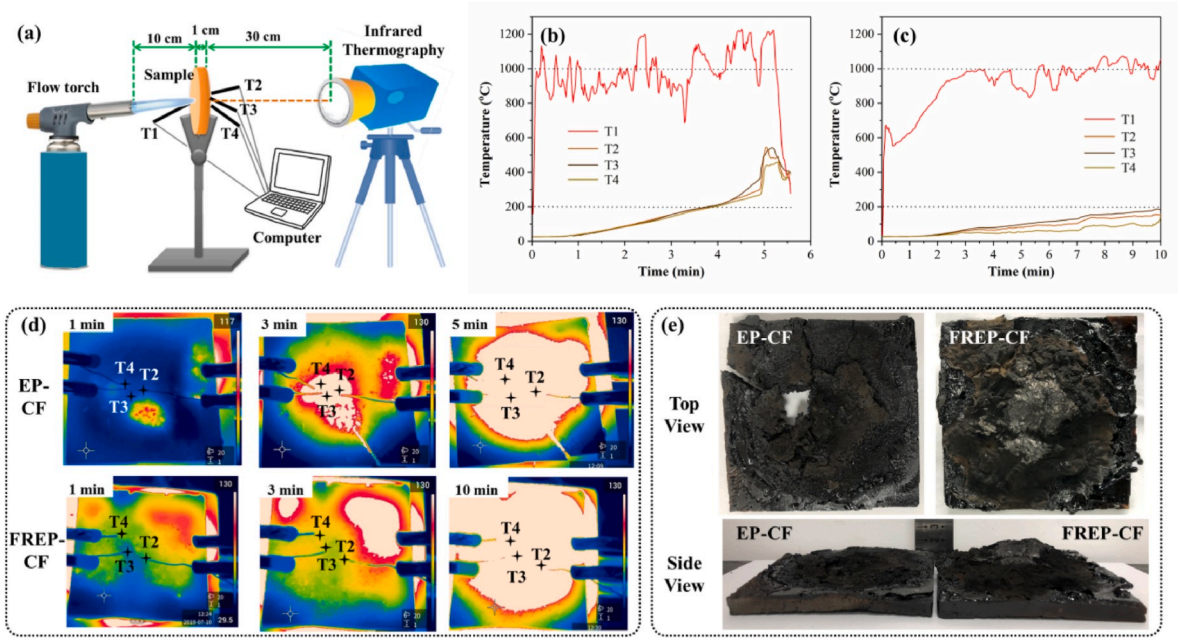

Fig. 8. (a) Diagrammatical illustration of the fire-resistant test. The time-dependent temperature profiles of the four reference points of (b) EP-CF and (c) FREP-CF (T1: the front side and T2-T4: the back side). (d) Thermographic images of the EP-CF and FREP-CF after being exposing to the flame at different times. (e) Digital photographs of the char residues of EP-CF and FREP-CF from top and side views.

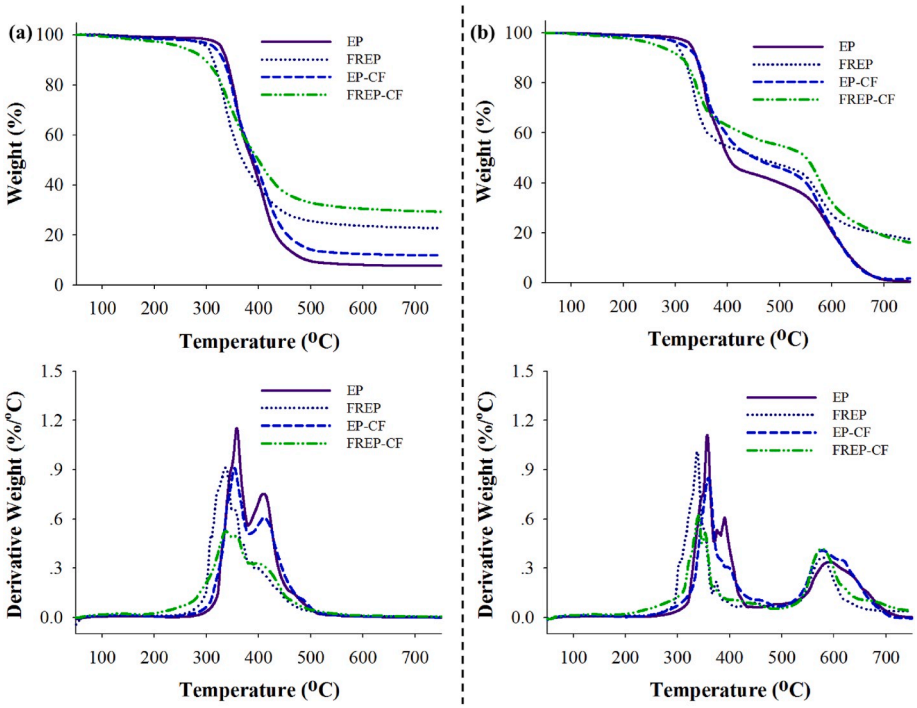

Fig. 9. TGA and DTG profiles of the samples: EP, FREP, EP-CF and FREP-CF under (a) nitrogen and (b) air atmosphere.

For the EP-CF, the outer char residue exhibits a continual char layer with numerous small holes that could retard the heat release to some extent (Fig. 10c-o), while the inner char layer shows a cellular structure with many cracks in the cell walls (Fig. 10c–i). Regarding the FREP-CF, a continual and compact surface is observed for the outer char (Fig. 10d-o), and a cellular structure with integrated cell walls is retained (Fig. 10d–i) that means better thermal resistance. Such a structured char is beneficial to suppressing the mass and heat transfer between decomposition zone and flame zone which accounts for the reduced heat release rate [59–61].

4. Conclusion

Highly flame retardant and effective EMI shielding epoxy composites were fabricated by impregnating pre-mixed liquid flame retardant and epoxy pre-polymer into a lignin-derived three-dimensional continuous carbon foam. SEM images showed that the voids of the carbon foams were filled with the flame-retardant epoxy resins without destroying

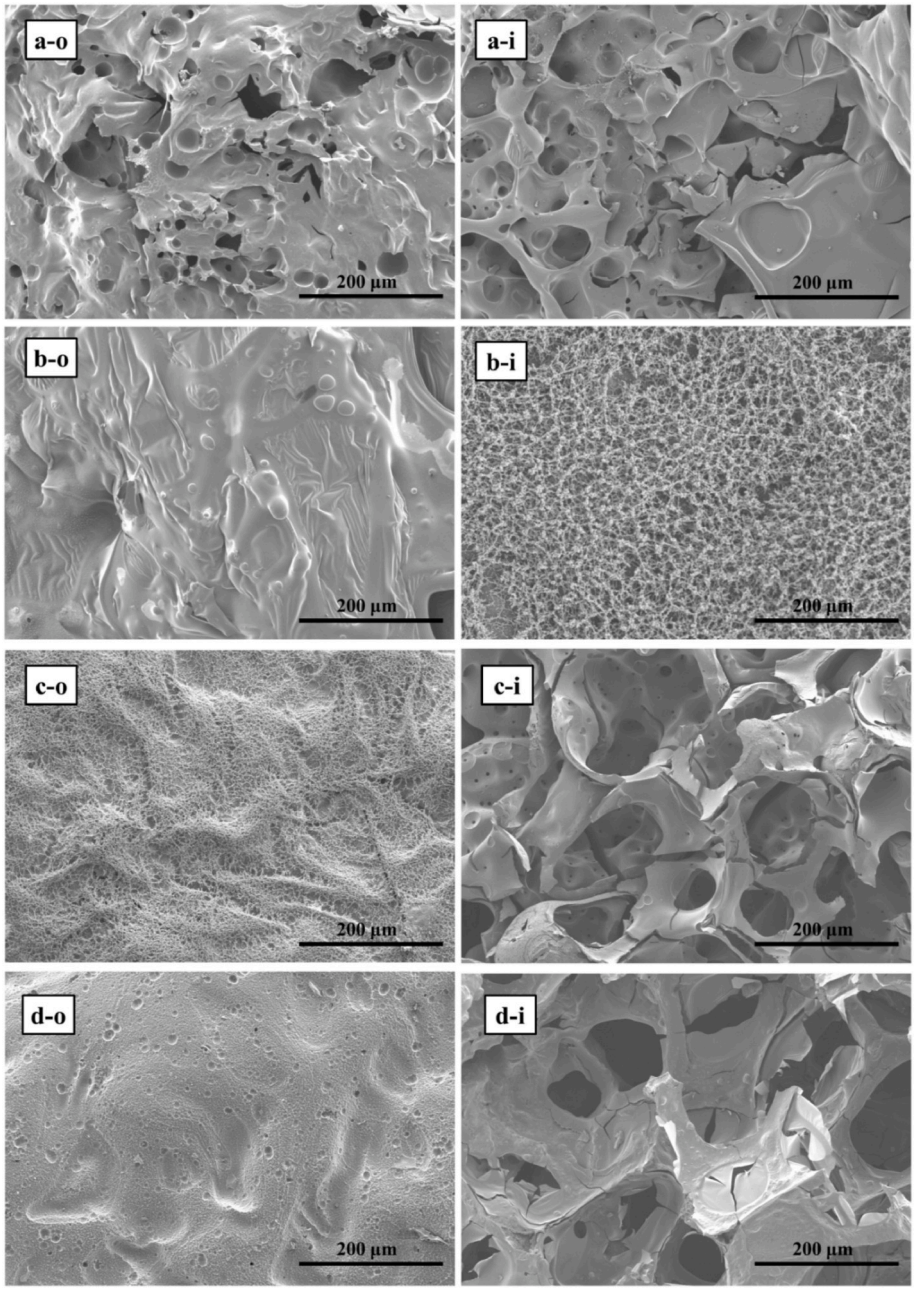

Fig. 10. SEM images of the char residues of (a) EP; (b) FREP; (c) EP-CF and (d) FREP-CF. Note: o: Outer part of the char; i: Inner part of the char.

their three-dimensional continuous microstructure. A relatively high electrical conductivity of 216 S/m and a remarkable EMI shielding effectiveness of approximately 33.5 dB were detected for the FREP-CF composite, which were much higher than the original epoxy matrix. Additionally, a LOI value of 29.5% as well as UL-94 V-0 rating is observed for the FREP-CF composite, whereas those are 23.0% and no rating for the EP-CF composite. The PHRR and the THR of the FREP-CF composite dropped by 64% and 37% measured by the cone calorimeter, respectively, compared to those of the original epoxy resin. Additionally, the FREP-CF composite can resist a high temperature flame (1000 °C) for 10 min with the temperature on the back side lower than 200 °C, which is superior over the EP-CF composite. The outstanding EMI shielding effectiveness is assigned to the formation of the three-dimensional interconnected networks for electron transport, while the significant flame retardancy enhancement is attributable to the formation of char layer that protect the underlying polymer from flame attack. This multifunctional epoxy composite combines low flammability, high ablation resistance, superior electrical conductivity and outstanding EMI shielding performances which enables it a promising candidate for electronics, aerospace and transportation applications.

Declaration of competing interest

The authors declare that they have no known competing financial interests or personal relationships that could have appeared to influence the work reported in this paper.

CRediT authorship contribution statement

Wenwen Guo: Investigation, Writing - original draft. **Yuyu Zhao:** Investigation. **Xin Wang:** Funding acquisition, Writing - review & editing. **Wei Cai:** Investigation. **Junling Wang:** Investigation. **Lei Song:**

Writing - review & editing. **Yuan Hu:** Supervision.

Acknowledgements

We gratefully acknowledge financial support from the National Natural Science Foundation of China (Grant No. 21604081), and the Open Project of State Key Laboratory Cultivation Base for Nonmetal Composites and Functional Materials (Grant No.: 16kffk03).

Appendix A. Supplementary data

Supplementary data to this article can be found online at https://doi.org/10.1016/j.compositesb.2020.107990.

References

[1] Zhou X, Qiu S, Xing W, Gangireddy CSR, Gui Z, Hu Y. Hierarchical polyphosphazene@molybdenum disulfide hybrid structure for enhancing the flame retardancy and mechanical property of epoxy resins. ACS Appl Mater Interfaces 2017;9:29147–56.
[2] Wang X, Hu Y, Song L, Xing W, Lu H, Lv P, et al. Flame retardancy and thermal degradation mechanism of epoxy resin composites based on a DOPO substituted organophosphorus oligomer. Polymer 2010;51:2435–45.
[3] Wang X, Hu Y, Song L, Yang H, Xing W, Lu H. Synthesis and characterization of a DOPO-substitued organophosphorus oligomer and its application in flame retardant epoxy resins. Prog Org Coating 2011;71:72–82.
[4] Kong Q, Wu T, Zhang J, Wang D-Y. Simultaneously improving flame retardancy and dynamic mechanical properties of epoxy resin nanocomposites through layered copper phenylphosphate. Compos Sci Technol 2018;154:136–44.
[5] Zhang Q, Wang J, Yang S, Cheng J, Ding G, Huo S. Facile construction of one-component intrinsic flame-retardant epoxy resin system with fast curing ability using imidazole-blocked bismaleimide. Compos B Eng 2019;177:107380.
[6] Cheng J, Wang J, Yang S, Zhang Q, Huo S, Zhang Q, et al. Benzimidazolyl-substituted cyclotriphosphazene derivative as latent flame-retardant curing agent for one-component epoxy resin system with excellent comprehensive performance. Compos B Eng 2019;177:107440.
[7] Perret B, Schartel B, Stöß K, Ciesielski M, Diederichs J, Döring M, et al. Novel DOPO-based flame retardants in high-performance carbon fibre epoxy composites for aviation. Eur Polym J 2011;47:1081–9.
[8] Yang S, Wang J, Huo S, Wang J, Tang Y. Synthesis of a phosphorus/nitrogen-containing compound based on maleimide and cyclotriphosphazene and its flame-retardant mechanism on epoxy resin. Polym Degrad Stabil 2016;126:9–16.
[9] Yang S, Wang J, Huo S, Wang M, Wang J, Zhang B. Synergistic flame-retardant effect of expandable graphite and phosphorus-containing compounds for epoxy resin: strong bonding of different carbon residues. Polym Degrad Stabil 2016;128:89–98.
[10] Yang S, Zhang Q, Hu Y. Synthesis of a novel flame retardant containing phosphorus, nitrogen and boron and its application in flame-retardant epoxy resin. Polym Degrad Stabil 2016;133:358–66.
[11] Wang X, Hu Y, Song L, Xing W, Lu H, Lv P, et al. Effect of a triazine ring-containing charring agent on fire retardancy and thermal degradation of intumescent flame retardant epoxy resins. Polym Adv Technol 2011;22:2480–7.
[12] Liu C, Chen T, Yuan CH, Song CF, Chang Y, Chen GR, et al. Modification of epoxy resin through the self-assembly of a surfactant-like multi-element flame retardant. J Mater Chem A 2016;4:3462–70.
[13] Martín C, Lligadas G, Ronda JC, Galià M, Cádiz V. Synthesis of novel boron-containing epoxy–novolac resins and properties of cured products. J Polym Sci, Part A: Polym Chem 2006;44:6332–44.
[14] Fang F, Ran S, Fang Z, Song P, Wang H. Improved flame resistance and thermo-mechanical properties of epoxy resin nanocomposites from functionalized graphene oxide via self-assembly in water. Compos B Eng 2019;165:406–16.
[15] Guo W, Wang X, Gangireddy CSR, Wang J, Pan Y, Xing W, et al. Cardanol derived benzoxazine in combination with boron-doped graphene toward simultaneously improved toughening and flame retardant epoxy composites. Compos Part A: Appl S 2019;116:13–23.
[16] Wang X, Kalali EN, Wan JT, Wang DY. Carbon-family materials for flame retardant polymeric materials. Prog Polym Sci 2017;69:22–46.
[17] Kalali EN, Wang X, Wang D-Y. Multifunctional intercalation in layered double hydroxide: toward multifunctional nanohybrids for epoxy resin. J Mater Chem A 2016;4:2147–57.
[18] Zhang J, Kong Q, Wang DY. Simultaneously improving the fire safety and mechanical properties of epoxy resin with Fe-CNTs via large-scale preparation. J Mater Chem A 2018;6:6376–86.
[19] Li X, Feng Y, Chen C, Ye Y, Zeng H, Qu H, et al. Highly thermally conductive flame retardant epoxy nanocomposites with multifunctional ionic liquid flame retardant-functionalized boron nitride nanosheets. J Mater Chem A 2018;6:20500–12.
[20] Yu B, Xing W, Guo W, Qiu S, Wang X, Lo S, et al. Thermal exfoliation of hexagonal boron nitride for effective enhancements on thermal stability, flame retardancy and smoke suppression of epoxy resin nanocomposites via sol–gel process. J Mater Chem A 2016;4:7330–40.
[21] Fu XL, Wang X, Xing W, Zhang P, Song L, Hu Y. Two-dimensional cardanol-derived zirconium phosphate hybrid as flame retardant and smoke suppressant for epoxy resin. Polym Degrad Stabil 2018;151:172–80.
[22] Wang X, Zhou S, Xing W, Yu B, Feng X, Song L, et al. Self-assembly of Ni–Fe layered double hydroxide/graphene hybrids for reducing fire hazard in epoxy composites. J Mater Chem A 2013;1:4383–90.
[23] Huang Y, Li N, Ma Y, Du F, Li F, He X, et al. The influence of single-walled carbon nanotube structure on the electromagnetic interference shielding efficiency of its epoxy composites. Carbon 2007;45:1614–21.
[24] Wang L, Qiu H, Liang C, Song P, Han Y, Han Y, et al. Electromagnetic interference shielding MWCNT-Fe3O4@Ag/epoxy nanocomposites with satisfactory thermal conductivity and high thermal stability. Carbon 2019;141:506–14.
[25] Song WL, Cao MS, Lu MM, Bi S, Wang CY, Liu J, et al. Flexible graphene/polymer composite films in sandwich structures for effective electromagnetic interference shielding. Carbon 2014;66:67–76.
[26] Wu J, Chen J, Zhao Y, Liu W, Zhang W. Effect of electrophoretic condition on the electromagnetic interference shielding performance of reduced graphene oxide-carbon fiber/epoxy resin composites. Compos B Eng 2016;105:167–75.
[27] Singh AP, Garg P, Alam F, Singh K, Mathur RB, Tandon RP, et al. Phenolic resin-based composite sheets filled with mixtures of reduced graphene oxide, γ-Fe_2O_3 and carbon fibers for excellent electromagnetic interference shielding in the X-band. Carbon 2012;50:3868–75.
[28] Chen Y, Zhang HB, Yang Y, Wang M, Cao A, Yu ZZ. High-performance epoxy nanocomposites reinforced with three-dimensional carbon nanotube sponge for electromagnetic interference shielding. Adv Funct Mater 2016;26:447–55.
[29] Gupta S, Tai NH. Carbon materials and their composites for electromagnetic interference shielding effectiveness in X-band. Carbon 2019;152:159–87.
[30] Chatterjee S, Saito T. Lignin-derived advanced carbon materials. ChemSusChem 2015;8:3941–58.
[31] Qu JY, Han Q, Gao F, Qiu JS. Carbon foams produced from lignin-phenol-formaldehyde resin for oil/water separation. N Carbon Mater 2017;32:86–91.
[32] Chen Y, Zhang H-B, Wang M, Qian X, Dasari A, Yu ZZ. Phenolic resin-enhanced three-dimensional graphene aerogels and their epoxy nanocomposites with high mechanical and electromagnetic interference shielding performances. Compos Sci Technol 2017;152:254–62.
[33] Kim J, Han NM, Kim J, Lee J, Kim JK, Jeon S. Highly conductive and fracture-resistant epoxy composite based on non-oxidized graphene flake aerogel. ACS Appl Mater Interfaces 2018;10:37507–16.
[34] Chen Z, Xu C, Ma C, Ren W, Cheng HM. Lightweight and flexible graphene foam composites for high-performance electromagnetic interference shielding. Adv Mater 2013;25:1296–300.
[35] Zeng Z, Jin H, Chen M, Li W, Zhou L, Zhang Z. Lightweight and anisotropic porous MWCNT/WPU composites for ultrahigh performance electromagnetic interference shielding. Adv Funct Mater 2016;26:303–10.
[36] García-Álvarez J, García-Garrido SE, Cadierno V. Iminophosphorane–phosphines: versatile ligands for homogeneous catalysis. J Organomet Chem 2014;751:792–808.
[37] Rebelo SLH, Guedes A, Szefczyk ME, Pereira AM, Araújo JP, Freire C. Progress in the Raman spectra analysis of covalently functionalized multiwalled carbon nanotubes: unraveling disorder in graphitic materials. Phys Chem Chem Phys 2016;18:12784–96.
[38] Wang X, Song L, Yang H, Xing W, Kandola B, Hu Y. Simultaneous reduction and surface functionalization of graphene oxide with POSS for reducing fire hazards in epoxy composites. J Mater Chem 2012;22:22037–43.
[39] Krämer RH, Zammarano M, Linteris GT, Gedde UW, Gilman JW. Heat release and structural collapse of flexible polyurethane foam. Polym Degrad Stabil 2010;95:1115–22.
[40] Yang H, Yu B, Song P, Maluk C, Wang H. Surface-coating engineering for flame retardant flexible polyurethane foams: a critical review. Compos B Eng 2019;176:107185.
[41] Zhang Y, Tian W, Liu L, Cheng W, Wang W, Liew KM, et al. Eco-friendly flame retardant and electromagnetic interference shielding cotton fabrics with multi-layered coatings. Chem Eng J 2019;372:1077–90.
[43] Mural PKS, Pawar SP, Jayanthi S, Madras G, Sood AK, Bose S. Engineering nanostructures by decorating magnetic nanoparticles onto graphene oxide sheets to shield electromagnetic radiations. ACS Appl Mater Interfaces 2015;7:16266–78.
[44] Phan CH, Mariatti M, Koh YH. Electromagnetic interference shielding performance of epoxy composites filled with multiwalled carbon nanotubes/manganese zinc ferrite hybrid fillers. J Magn Magn Mater 2016;401:472–8.
[45] Liang J, Wang Y, Huang Y, Ma Y, Liu Z, Cai J, et al. Electromagnetic interference shielding of graphene/epoxy composites. Carbon 2009;47:922–5.
[46] Aal NA, El-Tantawy F, Al-Hajry A, Bououdina M. New antistatic charge and electromagnetic shielding effectiveness from conductive epoxy resin/plasticized carbon black composites. Polym Compos 2008;29:125–32.
[47] Chen Y, Zhang HB, Huang Y, Jiang Y, Zheng WG, Yu ZZ. Magnetic and electrically conductive epoxy/graphene/carbonyl iron nanocomposites for efficient electromagnetic interference shielding. Compos Sci Technol 2015;118:178–85.
[48] Liang C, Qiu H, Han Y, Gu H, Song P, Wang L, et al. Superior electromagnetic interference shielding 3D graphene nanoplatelets/reduced graphene oxide foam/epoxy nanocomposites with high thermal conductivity. J Mater Chem C 2019;7:2725–33.
[49] Wu J, Ye Z, Ge H, Chen J, Liu W, Liu Z. Modified carbon fiber/magnetic graphene/epoxy composites with synergistic effect for electromagnetic interference shielding over broad frequency band. J Colloid Interface Sci 2017;506:217–26.

[50] Li J, Zhang G, Zhang H, Fan X, Zhou L, Shang Z, et al. Electrical conductivity and electromagnetic interference shielding of epoxy nanocomposite foams containing functionalized multi-wall carbon nanotubes. Appl Surf Sci 2018;428:7–16.
[51] Hashemi SA, Mousavi SM, Arjmand M, Yan N, Sundararaj U. Electrified single-walled carbon nanotube/epoxy nanocomposite via vacuum shock technique: effect of alignment on electrical conductivity and electromagnetic interference shielding. Polym Compos 2018;39:E1139–48.
[52] Yu B, Tawiah B, Wang LQ, Yin Yuen AC, Zhang ZC, Shen LL, et al. Interface decoration of exfoliated MXene ultra-thin nanosheets for fire and smoke suppressions of thermoplastic polyurethane elastomer. J Hazard Mater 2019;374:110–9.
[53] Lin B, Yuen ACY, Li A, Zhang Y, Chen TBY, Yu B, et al. MXene/chitosan nanocoating for flexible polyurethane foam towards remarkable fire hazards reductions. J Hazard Mater 2020;381:120952.
[54] Cai W, Mu X, Pan Y, Li Z, Wang J, Zhou X, et al. Black phosphorous nanosheets: a novel solar vapor generator. Sol RRL 2020:1900537.
[55] Wang X, Kalali EN, Wang DY. Renewable cardanol-based surfactant modified layered double hydroxide as a flame retardant for epoxy resin. ACS Sustainable Chem Eng 2015;3:3281–90.
[56] Wang X, Zhou S, Guo WW, Wang PL, Xing W, Song L, et al. Renewable cardanol-based phosphate as a flame retardant toughening agent for epoxy resins. ACS Sustainable Chem Eng 2017;5:3409–16.
[57] Shi Y, Yu B, Zheng Y, Yang J, Duan Z, Hu Y. Design of reduced graphene oxide decorated with DOPO-phosphanomidate for enhanced fire safety of epoxy resin. J Colloid Interface Sci 2018;521:160–71.
[58] Cai W, Hu Y, Pan Y, Zhou X, Chu F, Han L, et al. Self-assembly followed by radical polymerization of ionic liquid for interfacial engineering of black phosphorus nanosheets: enhancing flame retardancy, toxic gas suppression and mechanical performance of polyurethane. J Colloid Interface Sci 2020;561:32–45.
[59] Wang J, Zhang D, Zhang Y, Cai W, Yao C, Hu Y, et al. Construction of multifunctional boron nitride nanosheet towards reducing toxic volatiles (CO and HCN) generation and fire hazard of thermoplastic polyurethane. J Hazard Mater 2019;362:482–94.
[60] Wang J, Ma C, Mu X, Cai W, Liu L, Zhou X, et al. Construction of multifunctional $MoSe_2$ hybrid towards the simultaneous improvements in fire safety and mechanical property of polymer. J Hazard Mater 2018;352:36–46.
[61] Shi Y, Liu C, Liu L, Fu L, Yu B, Lv Y, et al. Strengthening, toughing and thermally stable ultra-thin MXene nanosheets/polypropylene nanocomposites via nanoconfinement. Chem Eng J 2019;378:122267.
[62] Huo SQ, Yang S, Wang J, Cheng JW, Zhang QQ, Hu YF, et al. A liquid phosphorus-containing imidazole derivative as flame-retardant curing agent for epoxy resin with enhanced thermal latency, mechanical, and flame-retardant performances. Journal of Hazardous Materials 2020;386:121984.
[63] Fang F, Huo SQ, Shen HF, Ran SY, Wang H, Song PA, et al. A bio-based ionic complex with different oxidation states of phosphorus for reducing flammability and smoke release of epoxy resins. Composites Communications 2020;17:104–8.